Order-Disorder Balance in Silk-Elastin-like Polypeptides Determines Their Self-Assembly into Hydrogel Networks

López Barreiro, Diego; Houben, Klaartje; Schouten, Olaf; Koenderink, Gijsje H.; Thies, Jens C.; Sagt, Cees M.J.

Important note
To cite this publication, please use the final published version (if applicable).
Please check the document version above.

Research Article

Order−Disorder Balance in Silk-Elastin-like Polypeptides Determines Their Self-Assembly into Hydrogel Networks

Diego López Barreiro,* Klaartje Houben, Olaf Schouten, Gijsje H. Koenderink, Jens C. Thies, and Cees M. J. Sagt

Read Online

ACCESS | Metrics & More | Article Recommendations | SI Supporting Information

ABSTRACT: The biofabrication of recombinant structural proteins with a range of mechanical or structural features usually relies on the generation of protein libraries displaying variations in terms of amino acid composition, block structure, molecular weight, or physical/chemical cross-linking sites. This approach, while highly successful in generating a wealth of knowledge regarding the links between design features and material properties, has some inherent limitations related to its low throughput. This slows down the pace of the development of *de novo* recombinant structural proteins. Here, we propose an approach to tune the viscoelastic properties of temperature-responsive hydrogels made of silk-elastin-like poly-peptides (SELPs) without modifying their sequence. To do so, we subject purified SELPs to two different postprocessing methods—water annealing or EtOH annealing—that alter the topology of highly disordered SELP networks via the formation of ordered intermolecular β-sheet physical cross-links. Combining different analytical techniques, we connect the order/disorder balance in SELPs with their gelling behavior. Furthermore, we show that introducing a functional block (in this case, a biomineralizing peptide) in the sequence of SELPs can disrupt its self-assembly and that such disruption can only be overcome by EtOH annealing. Our results suggest that postprocessing of as-purified SELPs might be a simple approach to tune the self-assembly of SELPs into biomaterials with bespoke viscoelastic properties beyond the traditional approach of developing SELP libraries via genetic engineering.

KEYWORDS: biofabrication, hydrogels, biomaterials, structural proteins, biopolymers, silk, elastin
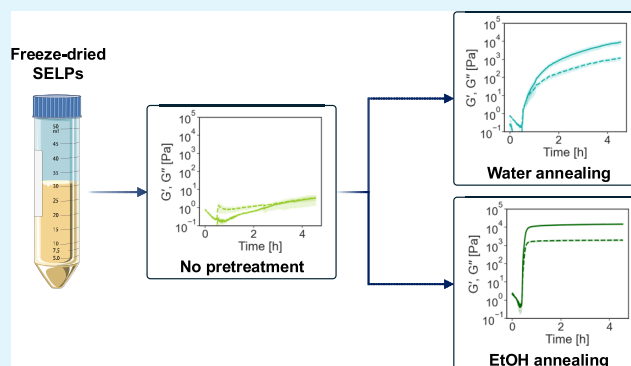
INTRODUCTION

Nature has evolved intricate mechanisms to direct the self-assembly of structural protein biopolymers from a disordered state into ordered, complex and functional materials such as bone, collagen, silk, elastin, or mussel threads.[1] These materials typically display impressive mechanical properties, a hierarchical structure, dynamic responsiveness, and environmental adaptability, that are conveyed by nano- and mesoscale motifs (e.g., β-sheets, helices, nanofibrils) encoded in the amino acid sequence of their constituent protein biopolymers.[2] Additional benefits of protein biopolymers include sustainability, ease of processability, and biodegradability. Oftentimes, the self-assembly of protein biopolymers into macroscopic materials involves a phase transition from disordered protein solutions into stable phase-separated condensates or fibers.[3] This phase transition can be tuned by controlling bottom-up interactions at the molecular scale (e.g., balance of ordered/disordered, hydrophobic/hydrophilic, or charged/neutral blocks in the protein sequence)[2] and top-down processing conditions (e.g., ionic strength, pH, shear).[4]

Inspired by these natural fabrication strategies, scientists are increasingly using structural protein biopolymers to manufacture synthetic self-assembling technical materials with applications in medicine, food, adhesives, textiles, or membrane technology, to name a few.[5−9] Protein biopolymers are normally harvested from animal sources (e.g., silk from silkworm cocoons, collagen from animal tissue, β-lactoglobulin from milk, lysozyme from egg whites), but these sources suffer from batch-to-batch variability, presence of contaminants, and cultural or religious concerns that limit their commercialization potential. Fortunately, developments in recombinant DNA technology and microbial bioprocesses allow us to overcome these issues and biomanufacture nonanimal-derived structural proteins. Additionally, recombinant DNA technology allows us

Table 1. Name, Amino Acid Sequence, and Theoretical MW of the SELP Library

name	sequence	theoretical MW (kDa)	experimental MW (kDa)
SE_{AI}	$[(IPAVG)_4[(VPGVG)_2(VPGIG)(VPGVG)_2]_4(GAGAGS)_4]_3$	34.9	34.8
bSE_{AI}	$[(IPAVG)_4[(VPGVG)_2(VPGIG)(VPGVG)_2]_2VTKHLNQISQSY[(VPGVG)_2(VPGIG)(VPGVG)_2]_2(GAGAGS)_4]_3$	39.1	39.2

to explore protein sequences beyond those selected for by evolution—we can now design entirely new structural proteins with properties inspired by natural structural proteins (e.g., the strength of silk, the stimuli-responsiveness of elastin, the stiffness of collagen), but that do not exist in nature.[10] This allows us to bring together the reproducibility of synthetic polymers with the biocompatibility and sustainability of natural biopolymers.[11]

Elastin-like polypeptides (ELPs) are an archetypical example of nature-inspired recombinant structural proteins. ELPs are intrinsically disordered polypeptides (IDPs) inspired by the VPGXG tandem repeats (being X any amino acid except proline) that confer thermoresponsiveness to natural tropoelastin.[12] ELPs have a reversible lower critical solution temperature (LCST) behavior, meaning that they are in a disordered water-soluble state below a transition temperature T_t, but coacervate and phase separate above it.[13] This thermoresponsiveness allows us to combine conformational freedom in the solvated state with the ability to create macromolecular hydrogel networks upon phase separation Furthermore, the thermoresponsiveness of ELPs allows us to purify them via temperature cycling, a scalable process that is cheaper than other protein purification methods like affinity chromatography.[14]

In nature, β-sheets act as physical cross-links to increase the strength of protein-based materials such as silk or amyloids.[15] This has inspired the fusion of elastin-like blocks (VPGXG) with silk-like blocks capable of forming β-sheets (GAGAGS) using recombinant DNA technology. This approach has led to the emergence of a broad class of proteins termed silk-elastin-like polypeptides (SELPs) that combine the stimuli-responsiveness of elastin-like blocks with the enhanced structural stability and mechanical properties of silk-like blocks.[16] SELPs hydrogels have found applications in areas like drug delivery, gene therapies, or tissue engineering.[17−23] However, the molecular mechanisms that regulate the structure, stimuli-responsiveness and viscoelastic properties of SELP hydrogels are still unclear. Recent studies have indicated that the assembly of silk-like β-sheets in SELP solutions above LCST is a thermodynamically controlled process that happens at a slower rate than the kinetically controlled coacervation of elastin-like blocks.[24] Coacervation above LCST brings silk-like blocks in close proximity, enabling their self-assembly into β-sheets that stabilize the transient and highly dynamic conformations of the elastin-like blocks.

Efforts to engineer the properties of SELP hydrogels have mostly focused on engineering their amino acid sequence, the molecular weight (MW) and/or the ratio of silk-like (ordered) to elastin-like (disordered) blocks.[16,24−26] This approach has also been applied to other recombinant structural proteins, such as squid-ring teeth proteins,[27] collagen-silk-like polypeptides,[28] resilin-like proteins,[29] or fusions of ELPs with partially ordered peptides.[30] This has enabled the manufacture of hydrogels with a wide range of sizes, morphologies, and mechanical properties, albeit at the expense of lengthy and costly design-build-test-learn (DBTL) cycles. Here, we

propose an alternative route to tune the mechanical and structural properties of SELP hydrogels. By subjecting purified SELPs to water annealing or ethanol (EtOH) annealing, we were able to alter the β-sheet content and thus the order/disorder balance in SELPs prior to hydrogel formation. This dramatically affected the ability of SELP solutions to form free-standing hydrogel networks above LCST. The effect of these post-treatments on the self-assembly of these proteins was assessed for two SELP variants: one containing only structural elastin- and silk-like blocks, and another containing also a functional peptide (in this case, a biomineralizing peptide). Our results bridge disorder-to-order transitions at the molecular scale, hierarchical self-assembly pathways, and macroscopic mechanical properties. In doing so, we demonstrated a previously unreported approach to engineer the viscoelasticity of SELPs hydrogels, manipulating the topology of the starting polymer network rather than the SELP amino acid sequence. This approach is simple and scalable and could accelerate the manufacture of SELP materials with a wider range of mechanical properties.

■ RESULTS AND DISCUSSION

Sequence Design, Expression, and Purification. The sequences of SELPs used in this study are shown in Table 1. SE_{AI} and bSE_{AI} were designed with a segmented copolymer structure that combined flexible/crystalline, structural/functional, and hydrophobic/hydrophilic blocks (Figure 1a). Both SELPs contained the same type and number of structural blocks, which were inspired by the sequences of tropoelastin (VPGVG, VPGIG, and IPAVG) and silk fibroin (GAGAGS). The high content in proline and glycine of elastin-like blocks promotes hydration and a disorder structure for SELPs, resulting in high conformational freedom and rubber-like elasticity.[16,31] VPGVG and VPGIG are inspired by the canonical ELP building block VPGXG[12] and display fully reversible thermoresponsiveness, whereas IPAVG leads to faster and kinetically arrested gelation[25,32] and displays hysteresis between solvation and desolvation. In turn, GAGAGS silk-like blocks can form ordered β-sheets that behave as intra- or intermolecular quasi-irreversible physical cross-links, enhancing the structural stability and mechanical properties of hydrogels. Additionally, we studied the effect of a functional (nonstructural) block on the self-assembly of SELPs. To do so, we introduced a hydrophilic block that has been reported to nucleate the biomineralization of hydroxyapatite (VTKHLNQISQSY)[33] into the structure of bSE_{AI}.

SE_{AI} and bSE_{AI} were recombinantly expressed in *E. coli* and purified via inverse transition cycling.[34] The purity of as-purified SELPs was confirmed via proton 1D solution nuclear magnetic resonance (NMR) (Figure 1b) by analyzing SELP solutions in D_2O at 295 K. The spectra confirmed the high purity of both SELPs, with sharp signals indicating a highly mobile protein backbone. The signals for both SELPs had a similar profile, with the exception of the signals for the biomineralizing block, which were only found in bSE_{AI}.
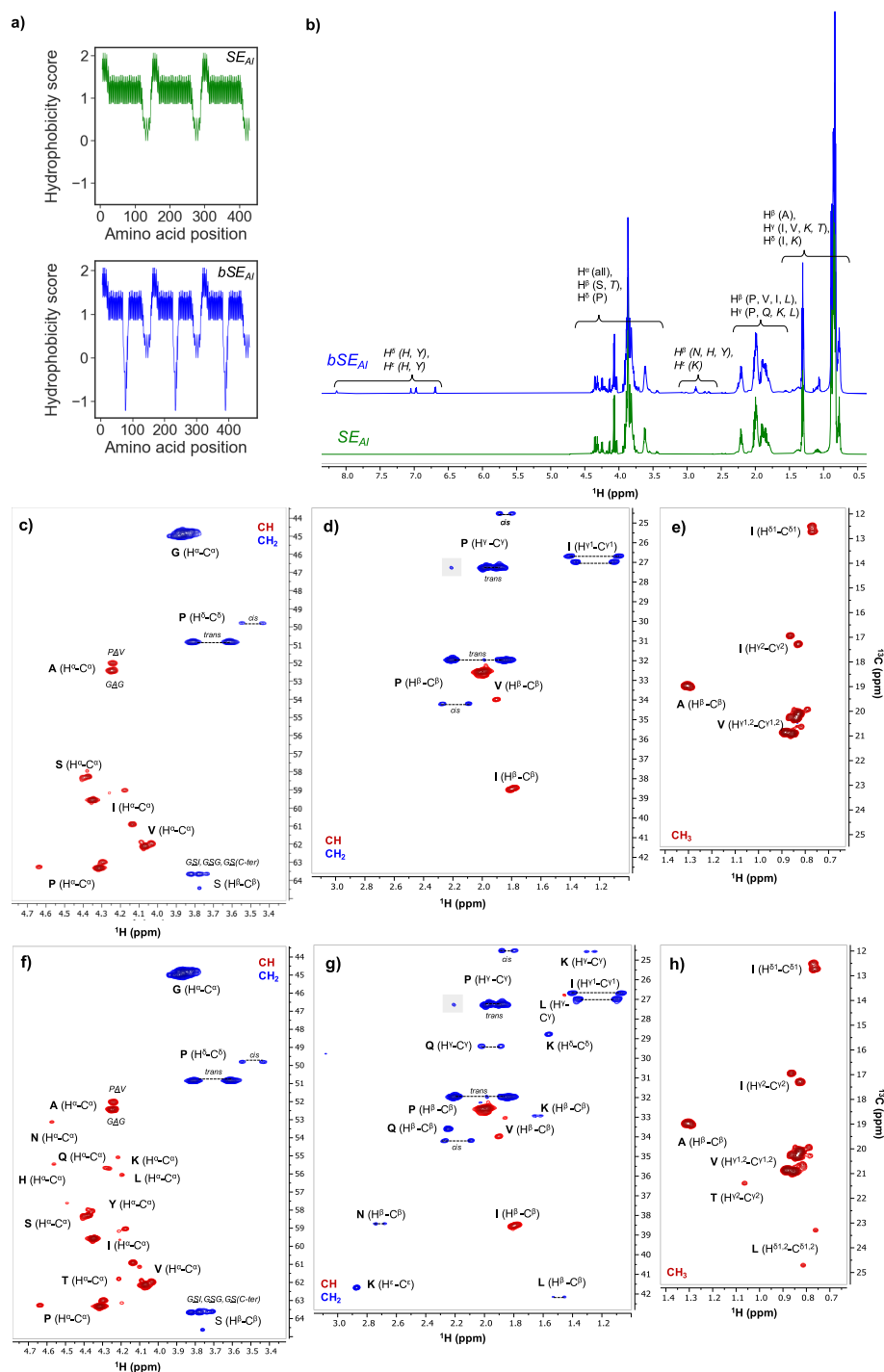
Figure 1. NMR spectra of solutions of freeze-dried SE$_{AI}$ and bSE$_{AI}$. (a) Hydropathy plots of the SELP sequences tested in this work as calculated using the Kyte-Doolittle scale. (b) 1D ^{1}H NMR spectra of SE$_{AI}$ (green, bottom) and bSE$_{AI}$ (blue, top) show highly pure proteins. Spectral regions are labeled with the specific protons that give signals in these regions, using labels $\alpha-\varepsilon$ to indicate the position in the amino acid and the amino acid one letter codes in normal font for the residues in elastin/silk-like blocks (V, I, S, G, A, P) and italic for the residues specific for the biomineralizing domain (H, Y, N, K, L, T, Q). (c-h) Zooms of the 2D edited ^{1}H−^{13}C HSQC spectra of SE$_{AI}$ (c-e) and bSE$_{AI}$ (f-h) show specific signals for residues in different blocks in the protein. Signals of CH and CH$_3$ groups are positive (red) and signals from CH$_2$ groups negative (blue). Spectral artifacts due to baseline distortions are indicated in gray. Thresholds of the different zooms have been adapted for clarity. Full spectra are shown in the Supporting Information.

Additional details were gathered via natural abundance 2D ^{1}H−^{13}C spectra (Figure 1c-h and Figures S1−S2). Signals were resolved through their adjacent carbon atom, resulting in a cross-peak at a specific ^{1}H and ^{13}C frequency. Interestingly, the 2D spectra of the two SELPs again overlapped perfectly for

amino acids in the common building blocks for both proteins. This indicated that the biomineralizing block did not alter the structure of the elastin-like and silk-like blocks. Putative assignment of the different cross-peaks was done using the chemical shifts for the different amino acids in a protein as
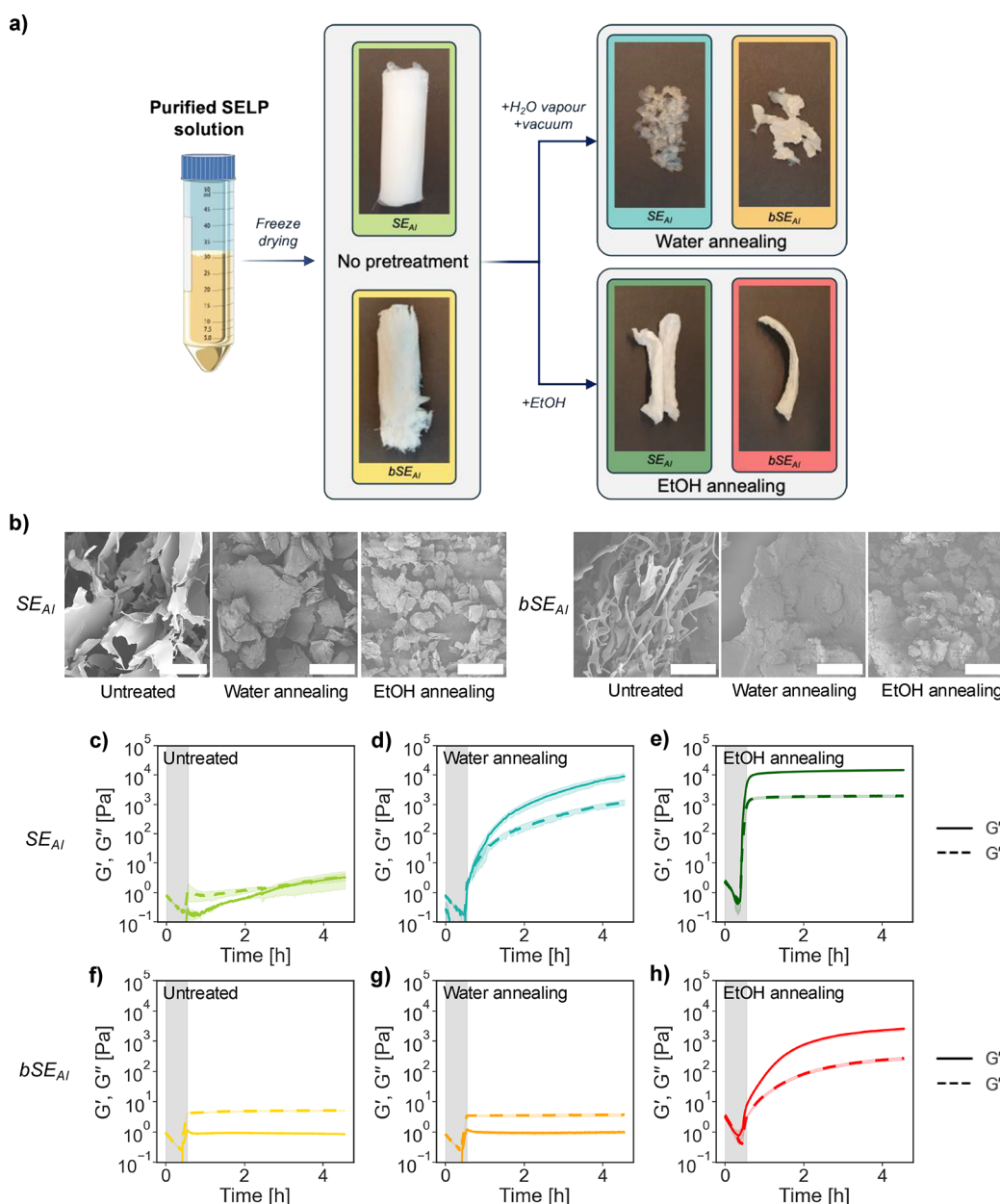
Figure 2. SELP formulations, macro- and microscopic appearance, and rheological properties. (a) Scheme of the different formulations tested in this work, with pictures of the resulting, dry material for each formulation. (b) SEM pictures of the microstructures for each SELP formulation (scale bar = 200 μm). (c-h) Rheological characterization (storage modulus G' and loss modulus G'') of SELP solutions in Milli-Q water (15 wt %) for untreated, water annealed and EtOH annealed samples during a temperature sweep between 4 and 37 °C (gray background) at a rate of 1 °C/min, followed by a time sweep at 37 °C for 4 h (white background) (n = 2).

provided by the Biological Magnetic Resonance Data Bank (BMRB)[35] and by Wang & Jardetzky.[36] Exact assignment of the cross-peaks for the H$^\alpha$-C$^\alpha$ region was challenging and labels were placed where the signals were expected. For other regions, cross-peaks could easily be attributed to a specific C−H couple in one of the amino acids. Purified SELPs were highly disordered in solution, as shown by the presence of chemical shifts typical of both cis and trans conformations (Figure 1d and 1h) in proline residues−a feature typical in elongated unstructured proteins.[37,38] Other residues also displayed multiple signals for their backbone and side-chain CH couples. For instance, two populations of alanine H$^\alpha$-C$^\alpha$ signals were observed, which were putatively assigned to alanine in either the PAV or GAG sequence (see Figure 1c and

1g for SE$_{AI}$ and bSE$_{AI}$, respectively). Similarly, valine residues also showed multiple signals, where especially the main cross-peak (2.0 and 32.5 ppm) for the H$^\beta$-C$^\beta$ correlation was compatible with valine in a random coil structure, while the minor signal at 1.9 and 34 ppm was compatible with valine in a sheet-like structure (Figure 1d and 1h).[36]

The properties of SE$_{AI}$ and bSE$_{AI}$ were tested in three different formulations: (1) untreated, (2) after postprocessing via water annealing and (3) after postprocessing via EtOH annealing. The water and EtOH annealing methods have been widely used to tune the amount of intermolecular β-sheet physical cross-links formed in silk-based materials after material synthesis.[39,40] Here we applied them to dry, purified SELPs prior to material synthesis. Our hypothesis was that by
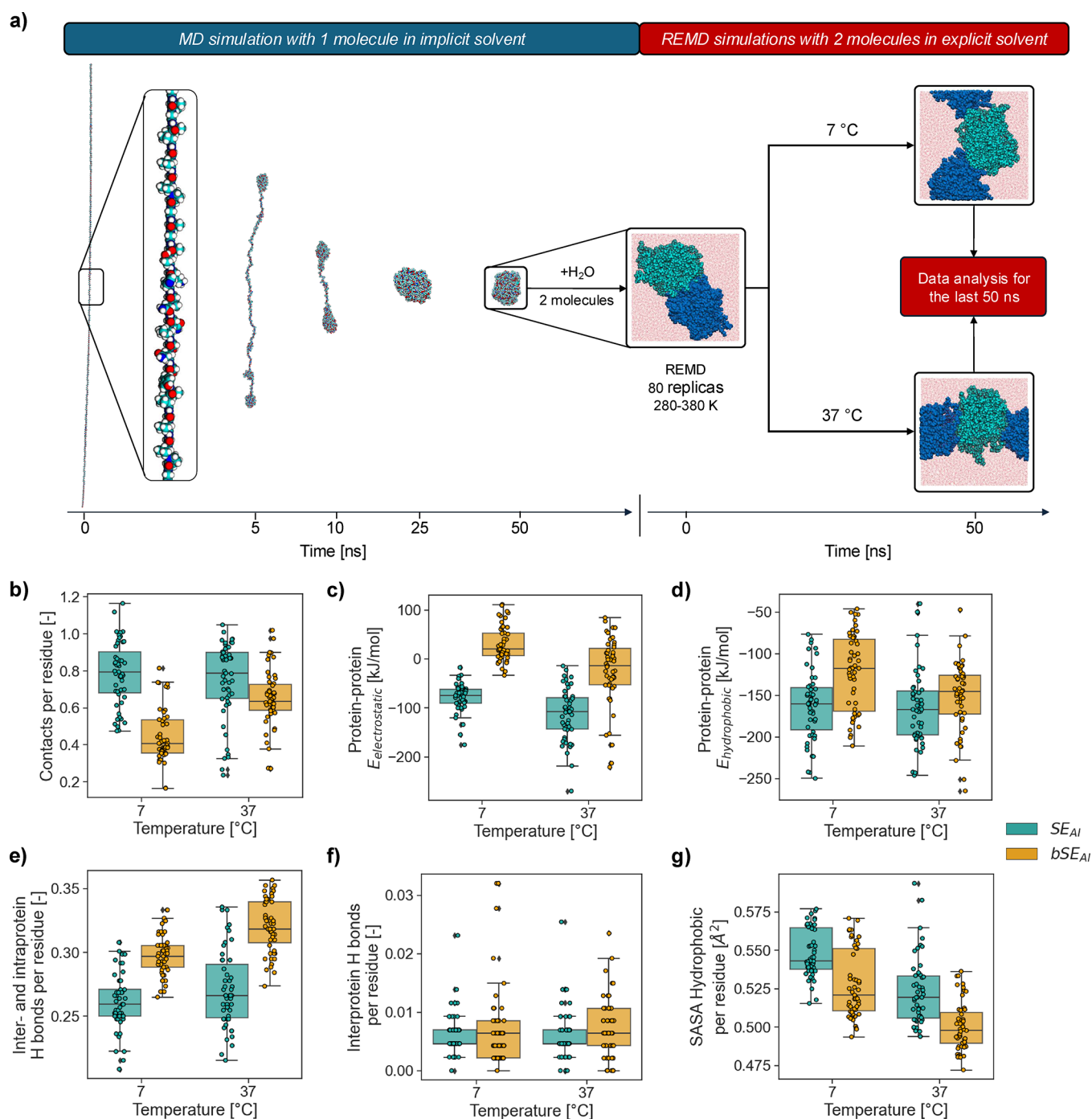
Figure 3. REMD simulations of SELPs. (a) Screenshots of the folding process (one chain in implicit solvent) and REMD simulations (two chains in explicit solvent) for bSE$_{AI}$. (b) Interprotein contacts normalized by the number of residues in each SELP. (c) Electrostatic interprotein interaction energy. (d) Hydrophobic interprotein interaction energy. (e) Total protein hydrogen bonds normalized by the number of residues in each SELP. (f) Interprotein hydrogen bonds normalized by the number of residues in each SELP. (g) Solvent accessible surface area of hydrophobic residues normalized by the number of residues in each SELP.

altering the content of β-sheets in these materials, we could tune their ability to form hydrogels in a thermoresponsive manner, as well as their viscoelastic properties. The three formulations tested in this work are displayed in Figure 2a, showing the clear changes in the physical appearance of SELPs caused by both types of annealing. Untreated SELPs were obtained directly after freeze-drying and displayed a porous structure with a spongy consistency. Conversely, water annealed and EtOH annealed samples became rigid and with

a plastic-like consistency. Annealing postprocessing heavily modified the microstructure of SELPs, as observed via SEM (Figure 2b), but did not alter their MW, as shown by SDS PAGE (Figure S3). Annealing also affected the solubility of SELPs in water: while untreated SELPs were fully soluble at concentrations in the range of 0.5−250 mg/mL, water and EtOH annealed SELPs required cryomilling to render them soluble in Milli-Q water.
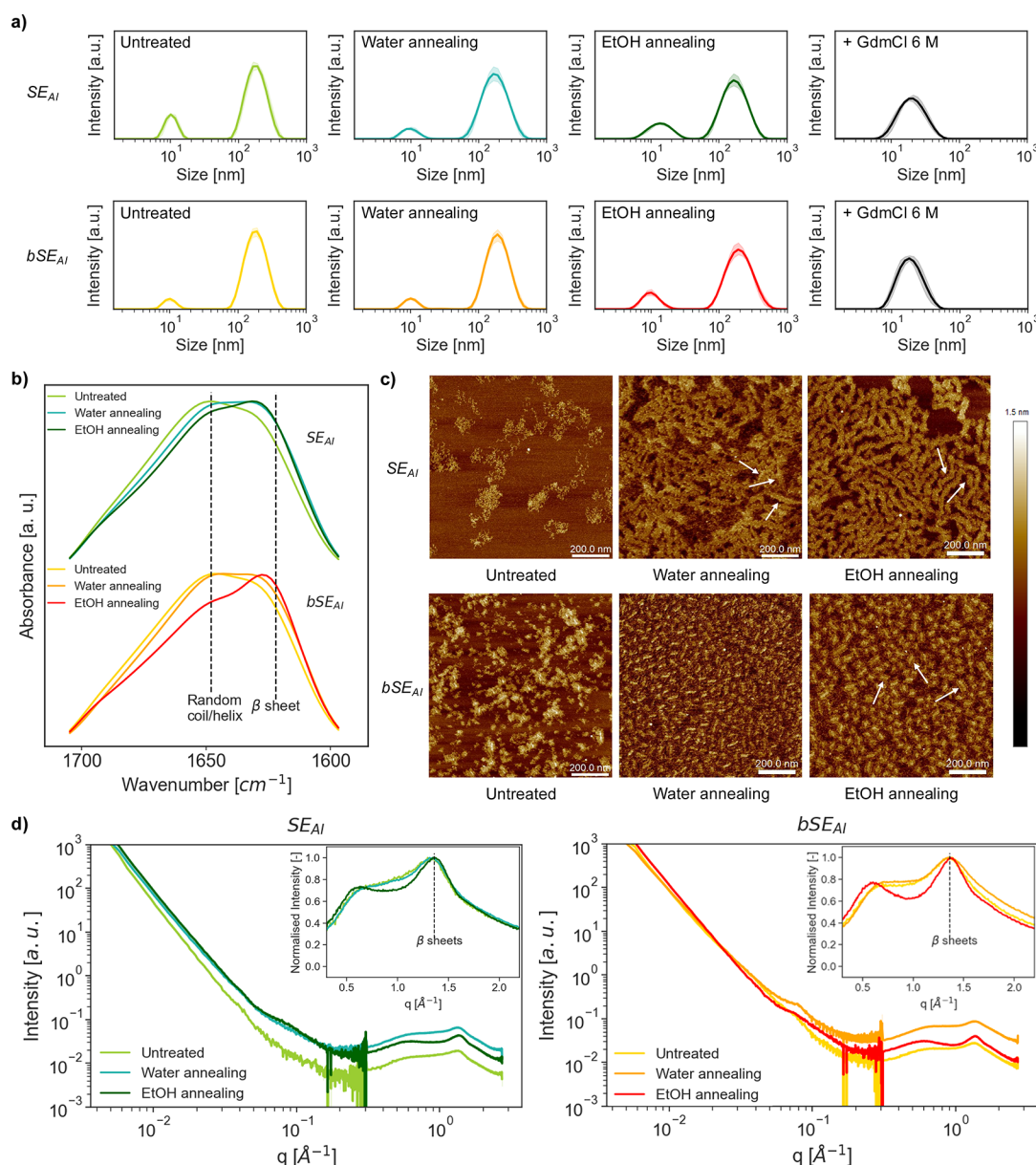
Figure 4. Characterization of the network structure of SELPs in different formulations. (a) Size distributions of the hydrodynamic radius (n = 5) of 0.5 mg/mL solutions in Milli-Q water of the different SELP formulations tested in this work. (b) Normalized FTIR spectra of the amide I region for dry SELP formulations (n = 2). (c) AFM images of SELP networks in different formulations, imaged in dried conditions on mica. (d) SAXS/WAXS patterns for SELPs. Insets represent the normalized diffraction pattern for WAXS measurements to facilitate the comparison in terms of β-sheet content for each formulation.

Rheology. The rheological behavior of SE_{AI} and bSE_{AI} solutions (15 wt %) was probed via small amplitude oscillatory rheology (Figure 2c-h). The linear viscoelastic (LVE) region of these solutions was determined via amplitude sweeps after 4 h of incubation at 37 °C (Figure S4). Most of the formulations showed a response independent of strain amplitude (0.01–15%). Only solutions from water annealed and EtOH annealed SE_{AI} showed a decrease at high amplitudes (above 1% for water annealed SE_{AI}, and above 8% for EtOH annealed SE_{AI}). SELP solutions were also subjected to a temperature ramp (1 °C/min) between 4 and 37 °C (gray background areas in Figures 2c–h), followed by a time sweep at 37 °C for 4 h (white background areas in Figures 2c–h). Untreated SE_{AI} showed a slow but steady increase in the storage modulus once the T_t was surpassed (Figure 2c). This was attributed to the

continuous formation of intermolecular β-sheets for SELP solutions above LCST. To confirm this, SE_{AI} solutions in 6 M GdmCl were assessed, due to the ability of GdmCl to disrupt β-sheets in protein networks.[41] Indeed, the addition 6 M GdmCl eliminated the increase in storage modulus over time above LCST (Figure S5), confirming that β-sheets (and not just protein entanglements) were the cause of the increase in modulus of untreated SE_{AI} solutions above LCST. Water-annealed SE_{AI} solutions showed a steady increase in G' during the temperature and time sweeps akin to that of untreated SE_{AI}, but at a much faster rate (Figure 2d). Finally, EtOH-annealed SE_{AI} solutions gelled instantly once T_t was surpassed, and its storage and loss moduli remained unchanged thereafter (Figure 2e). These data confirms that postprocessing indeed

altered the ability of SE$_{AI}$ solutions to self-assemble into percolated hydrogel networks above T$_t$.

The self-assembly of bSE$_{AI}$ was negatively impacted by the presence of the hydrophilic biomineralizing functional block. Untreated and water-annealed bSE$_{AI}$ were unable to gel after 4 h at 37 °C. (Figure 2f,g) Furthermore, unlike SE$_{AI}$, the storage modulus (G') of bSE$_{AI}$ solutions only increased until T$_t$ was surpassed, remaining constant and lower than the loss modulus (G'') thereafter. Only EtOH annealing rendered bSE$_{AI}$ able to gel, with a gelling profile similar to that of water annealed SE$_{AI}$ (Figure 2h). The different formulations tested here also led to wide variations in the stress relaxation spectra of SELP solutions (Figure S6). The solutions that were unable to gel exhibited a dependence of the shear moduli with frequency, likely due to the ability of those networks to relax entanglements because of their low content in intermolecular β-sheets.

To investigate the differences in gelation between SE$_{AI}$ and bSE$_{AI}$, replica exchange molecular dynamics (REMD) simulations were performed. These simulations aimed to capture the differences in interchain interactions of elastin-like blocks in both SELPs below T$_t$ (7 °C) and above T$_t$ (37 °C). Effects arising from the water or EtOH annealing post-treatments were not considered in these simulations, as those post-treatments aimed at controlling the formation of β-sheets via silk blocks but are not expected to affect the thermoresponsiveness of elastin-like blocks. REMD simulations were performed with systems consisting of two molecules of SE$_{AI}$ or bSE$_{AI}$ (Figure 3a). Overall, the simulations indicated a lower propensity of bSE$_{AI}$ to interact with neighboring chains. SE$_{AI}$ molecules had a higher propensity to form contacts with each other than bSE$_{AI}$, especially at 7 °C (Figure 3b). These contacts (defined as α carbons in the backbone of different SELP chains located less than 10 Å apart) are a necessary step for the formation of interprotein β-sheets, which are critical for the formation of robust hydrogel networks in SELPs. The higher stability of SE$_{AI}$-SE$_{AI}$ interactions was also shown by their more negative values of the electrostatic interaction energies (and to a lesser extent hydrophobic interaction energies too) (Figures 3c-d). Additionally, bSE$_{AI}$-bSE$_{AI}$ systems formed more hydrogen bonds (normalized by the number of residues of each SELP) (Figure 3e). However, the number of interprotein hydrogen bonds was similar for both systems (Figure 3f), indicating that the increase in hydrogen bonding in bSE$_{AI}$-bSE$_{AI}$ systems was due to intraprotein hydrogen bonds. Additionally, the solvent accessible surface area (SASA) of hydrophobic amino acids was lower for bSE$_{AI}$ (Figure 3g). A lower SASA for hydrophobic amino acids is detrimental for the formation of robust SELP hydrogels, as contacts between hydrophobic amino acids are key for the coacervation of elastin-like blocks.[31,42]

Network Structure. The SELPs solutions described in Figure 2c were all prepared in the same manner: dry SELPs were dissolved in Milli-Q water (15 wt %), incubated on ice for 10 min with occasional stirring, and subsequently analyzed by small amplitude oscillatory rheology. This suggested that the variations in the behavior of each formulation must arise from features already present in the dry SELPs. To test this idea, we applied a range of analytical techniques, including DLS, FTIR, AFM, SAXS, and WAXS.

The hydrodynamic diameter D_h of SE$_{AI}$ or bSE$_{AI}$ was assessed via DLS using diluted solutions (0.5 mg/mL) (Figure

4a). Before analysis, the samples were passed through a 0.2 μm syringe filter to remove any dust particles, followed by an equilibration at 25 °C (below T$_t$) for 5 min. The solutions showed a peak in the range of the expected values for the D_h of single IDP molecules in solution (10.9 nm for SE$_{AI}$ and 11.4 nm for bSE$_{AI}$). Surprisingly, all samples contained a second, more intense peak at higher D_h values, an effect previously observed for other SELPs.[43] Unfortunately, the reason for this (given that the samples passed through a 0.2 μm filter before analysis) remains unclear at this stage. We hypothesize the larger D_h values might originate from intermolecular β-sheets that could form below T$_t$ due to the shearing flow in the syringe filter, or from random contacts between silk-like blocks in solution. One argument that supports this hypothesis is that SELP solutions in GdmCl 6 M do not exhibit such large particles. We consider it unlikely that these aggregates arise from the thermoresponsive aggregation of SELPs, because these experiments were carried out below T$_t$.

We next tested the effect of the SELP formulation (untreated, water-annealed, or EtOH-annealed) on its secondary structure via Fourier Transform Infrared (FTIR) spectroscopy (Figure 4b, full spectra in Figure S7). The annealing postprocessing caused a shift of the amide I band toward the region around ca. 1620 cm^{-1}, a fingerprint of the formation β-sheets in protein materials.[44] The prominence of the β-sheets band followed the order untreated < water annealing < EtOH annealing for both SELPs. Nonetheless, despite the increasing content in β-sheets, the polymers retained a significant fraction of disordered regions, as shown by peak/shoulder at around 1650 cm^{-1}. The effect of postprocessing was also clearly visible via AFM imaging (Figure 4c and Figure S8). Both SE$_{AI}$ and bSE$_{AI}$ without postprocessing contained isolated clusters of disordered protein chains. In turn, water and EtOH annealing caused the emergence of fibrillar structures formed by stacked layers perpendicular to the direction of the fiber (as exemplified by the arrows displayed in Figure 4c). The change in direction of those arrows evidenced that the observed layered structures did not arise from artifacts due to the scanning direction of the tip. Notably, the growth of those stacked structures was affected by the type of SELPs: while SE$_{AI}$ was able to form long fibrillar structures, bSE$_{AI}$ did not grow beyond small wormlike micelles. The type of annealing affected the morphology of those fibers: EtOH annealing formed longer fibers in SE$_{AI}$, and wormlike micelles of a higher radius in bSE$_{AI}$. Furthermore, water-annealed SE$_{AI}$ samples also showed the presence of a significant amount of small fibrillar structures (Figure S9) that were not present in EtOH-annealed samples. This hinted that EtOH annealing was more effective in forming β-sheets (as indicated also by FTIR), resulting in a network with higher connectivity and a more ordered structure.

X-ray scattering was used to gain further insight into the nanoscale structures present in dry SELPs. As expected, WAXS diffraction patterns confirmed the presence of ordered β-sheet regions in all the samples analyzed (Figure 4d). The presence of diffuse rings in the 2D WAXS patterns was consistent with the polymers being mainly disordered and without a preferential orientation for the β-sheet regions (Figure S10). Radial integration of the 2D scattering profiles showed a peak at q = 1.30−1.38 Å^{-1} for all formulations in both SELPs. According to the Bragg expression,[45] this corresponded to d = 2π/q = 4.55−4.85 Å, which was within the typical range of distances reported for adjacent β-strands in crystalline regions
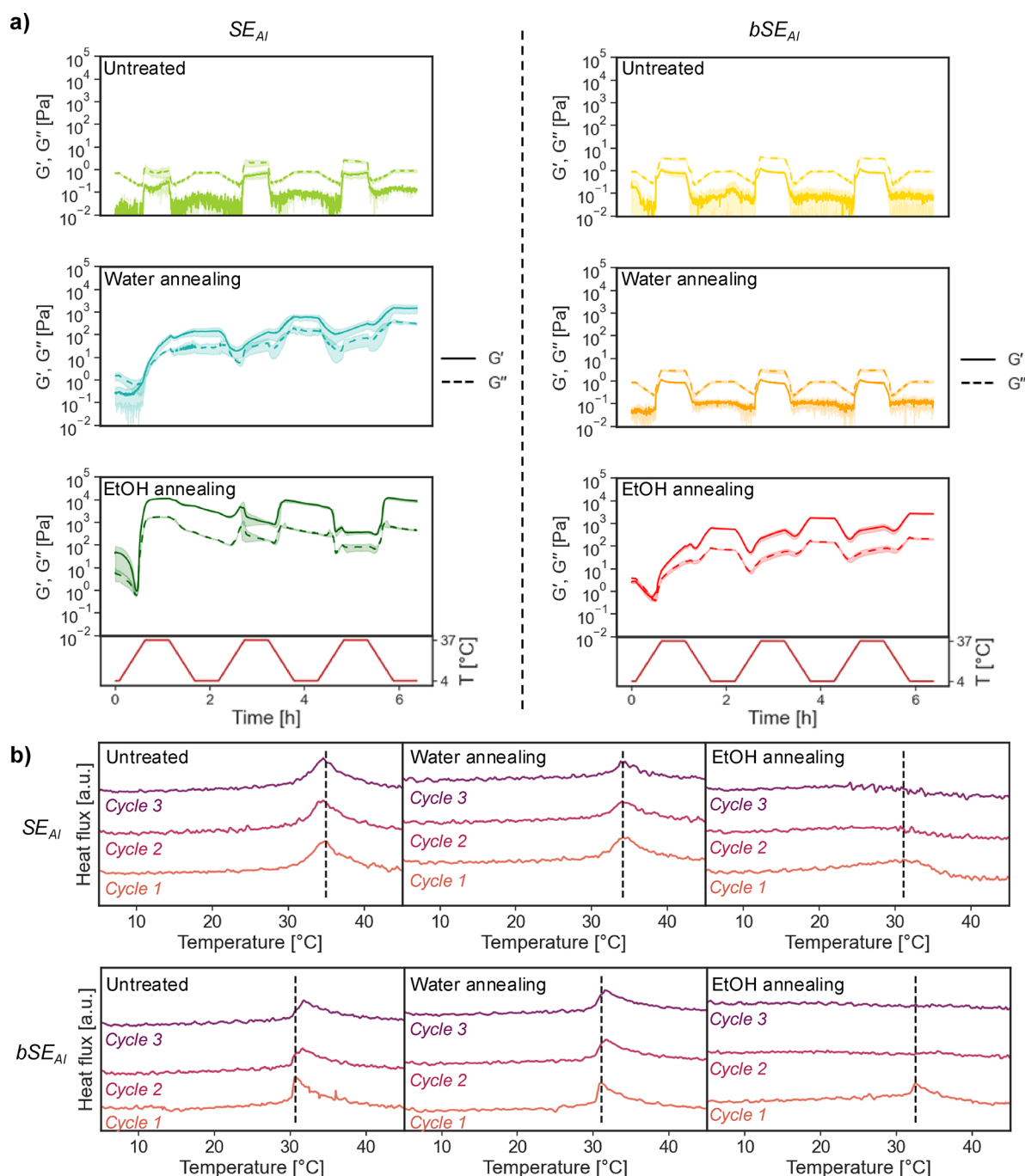
Figure 5. Influence of the formulation on the reversible gelation of SELPs. (a) Thermal cycling between 4 and 37 °C of SELP solutions (15 wt %) at a heating/cooling rate of 1 °C/min (f = 1 Hz, γ = 0.3%), with 30 min of resting time between temperature ramps (n = 2, SE_{AI} on the left column, bSE_{AI} on the right column). (b) Thermograms for 3 thermal cycles between 4 and 50 °C (1 °C/min) of SELP solutions (15 wt %). Y-axis is offset for clarity. The vertical dashed line indicates the location of the thermogram maximum (associated with the T_t) for cycle 1.

for protein materials.[46−48] Similar patterns were reported for other protein-based materials, such as silk-amyloid fusions,[49] whey-PHPA elastomers,[50] tropoelastin-based materials[51] or plant-based thermosetting materials.[46] The increased sharpness of the peak at q = 1.30−1.38 Å^{-1} for water- and EtOH-annealed samples again confirmed the higher content of β-sheets in these materials. The annealing postprocessing did alter the content in β-sheet crystals, but only caused small variations in their size. The monotonic decrease with increasing wavenumber q of the SAXS intensity curves of SE_{AI} and bSE_{AI} and their lack of marked diffraction peaks

(Figure 4d and Figure S11) again confirms that both materials were also mainly disordered and had no characteristic length scale, regardless of the formulation under consideration. Only a small shoulder at q ∼ 0.07 Å^{-1} was observed in annealed samples, which could be attributed to the formation of nanocrystalline domains.

Taken together, the results from different analytical techniques provide a picture of how postprocessing routes can be leveraged to tune nanoscale features (i.e., intermolecular β-sheets) in SELPs, and how those features influence the macroscopic gelation of SELP solutions. Untreated SELPs

in solution were highly flexible and had limited connectivity. As a result, they phase-separated above T_t but could not form a cohesive network. Water- or EtOH-annealed SELPs had an increased content in intermolecular β-sheets. These β-sheets appeared to catalyze the self-assembly of additional β-sheet, especially above T_t thanks to the coacervation of elastin-like blocks. This would explain the increase in storage modulus observed for water-annealed SE_{AI} or EtOH-annealed SE_{AI} and bSE_{AI} (compared to untreated formulations). The rate at which new β-sheets formed above T_t appeared to be influenced controlled by the initial content of β-sheets in dry SELPs. As more β-sheets formed, they stabilized the nascent hydrogel network via strong hydrogen bonding, until a saturation level was achieved. This would be consistent with nucleation-aggregation logistic mechanisms akin to those proposed for the self-assembly for natural and synthetic silk materials:[48,52,53] the higher the β-sheet content in the starting material, the faster the saturation level is achieved.

Overall, the data suggests the existence of a percolation threshold in the connectivity of SELP chains via β-sheets above which SELP solutions at $T > T_t$ can form a robust hydrogel. Given that SELPs are typically purified using alternating low-temperature and high-temperature cycles, our results under-score how β-sheets formed between silk-blocks during the high-temperature cycles can dramatically impact the gelling behavior and the viscoelastic properties of SELP materials. Moreover, the properties of SELPs have been traditionally tuned by modifying the sequence, MW or block composition.[16,24,43] However, such an approach requires long DBTL cycles of gene synthesis, transformation, protein expression and purification, before the effect of those modifications can be evaluated. Our results hint at a simpler and controllable strategy to tune the gelling propensity of SELPs—by merely adjusting the amount of β-sheets in the starting material via water or EtOH annealing—that could accelerate DBTL cycles for new protein-based materials.

Reversibility. We assessed the reversibility of the gelation of SELP solutions over three temperature cycles between 4 and 37 °C, with a resting time of 30 min after each temperature ramp (Figure 5a). In previous studies, we described the fully reversible gelation for ELP solutions with the same concentration.[25] A similar behavior was described elsewhere when cycling SELP solutions too, but only for a few temperature cycles.[43] Once the number of cycles increased (>10 cycles), the thermoresponsiveness of SELP hydrogels disappeared. In our work, the reversibility of the gelation for the SELP solutions was strongly dependent on the initial amount of β-sheets and the presence of a biomineralizing block. Untreated SE_{AI} and bSE_{AI} were unable to gel after three temperature cycles, with $G'' > G'$ throughout. Water-annealed SE_{AI} showed an onset for the gelation once T_t was surpassed during the first ramp. From that point onward, a network formed and G' dominated over G'' regardless of the temperature, even during cooling ramps, and the moduli increased with every heating ramp from 4 to 37 °C. In turn, water-annealed bSE_{AI} was unable to gel after three temperature cycles, demonstrating the deleterious effect of the biominer-alizing block for self-assembly. EtOH-annealed samples gelled during the first heating ramp for both SE_{AI} and bSE_{AI}. However, their behavior in subsequent cycles was different. SE_{AI} achieved its maximum G' as soon as T_t was surpassed in the first heating ramp, whereas bSE_{AI} kept increasing its moduli during the three cycles.

Notably, a loss of the thermoresponsiveness was observed for EtOH-annealed SE_{AI} solutions after the first temperature cycle. In fact, EtOH annealed SE_{AI} networks became softer above T_t during the second temperature ramp between 4 and 37 °C. This was different from the typical behavior of solutions with LCST-like behavior, which are normally softer below T_t than above it. A possible explanation for this behavior is provided by the theory of energy landscape:[54,55] flexible elastin-like blocks are able to explore many local energy minima due to their conformational freedom, whereas silk-like blocks evolve toward global energy minima represented by β-sheets. Once the amount of intermolecular β-sheets reaches a critical threshold, they impose a high energy barrier on the conformational freedom of elastin-like block. Thus, we hypothesize that EtOH annealed SE_{AI} networks fully developed during the first temperature cycle, reaching a saturation value for the β-sheets content that restricted the conformational freedom of elastin-like blocks, effectively erasing their thermoresponsive behavior. The resulting behavior was more akin to that of rubbers, in which higher temperatures cause a relaxation of entanglements that weakens their mechanical properties.[50] We also observed that the biomineralizing blocks in bSE_{AI} solutions hindered their self-assembly into robust hydrogels, delaying the formation of a fully developed network. We hypothesize that this could be prevented in future DBTL cycles by changing the location of the biomineralizing blocks, for instance by placing them at the ends of the SELPs—rather than regularly distributing them throughout the sequence.

The reversibility of gelation was also analyzed via DSC, cycling 15 wt % solutions of the various SE_{AI} and bSE_{AI} formulations between 4 and 50 °C for three times (Figure 5b). The thermograms for untreated SE_{AI} and bSE_{AI} showed a similar behavior, with a peak at around 35 °C arising from the T_t and consequent coacervation of elastin-like blocks. In water-annealed samples, the first cycle had a more prominent peak than the subsequent cycles, especially for SE_{AI}. This indicated that an initial hydrogel network formed during the first cycle, and that every subsequent cycle progressively decreased the thermoresponsiveness of elastin-blocks (as shown by the decreasing the intensity of the peak associated with T_t). For EtOH-annealed samples, the T_t peak was only present in the first cycle. The thermogram of subsequent cycles displayed a flat profile, indicating that the thermoresponsiveness of elastin-like blocks disappeared. Overall, the rheology and DSC results underscored the critical role of silk-like blocks not only in controlling the robustness of SELP hydrogel networks, but also their thermoresponsiveness.

■ CONCLUSIONS

The genetic basis of sequence and length control in SELPs has resulted in a wealth of studies that investigate the effect of amino acid composition, MW, block composition or physical/chemical cross-linking strategies on the gelation of SELP solutions. Here we proposed an alternative route to tune the viscoelasticity and gelling propensity of SELP solutions by applying a postprocessing step (water annealing or EtOH annealing). These postprocessing steps significantly altered dry SELPs after purification, influencing their connectivity via intermolecular β-sheets, which also impacted the gelling propensity. Using molecular, micro-, and mesoscale exper-imental and computational characterization techniques, we provided a comprehensive view of the complex crosstalk

between ordered silk-like blocks and flexible and stimuli-responsive elastin-blocks. Water and EtOH annealing increased the β-sheet content in SELPs, with the higher content of β-sheets in EtOH-annealed samples enhancing their ability to gel. Our results also underscored the deleterious effect of a functional building block (in this case, a biomineralization block) on the gelation of SELPs. The postprocessing methods used here did not require the use of toxic solvents, covalent cross-linkers, or nonbiodegradable materials. Moreover, they provided a facile top-down approach to direct the bottom-up self-assembly of SELPs. Overall, this work suggests a new route to tune the supramolecular self-assembly of SELPs by tuning the order−disorder balance after protein purification, rather than by sequence engineering. While this approach is demonstrated here for SELPs, it could be applicable to other protein-based materials that rely on β-sheets to control their mechanical properties, such as materials derived from plant proteins[56] or squid ring teeth proteins.[57]

■ METHODS

Synthesis and Microbial Production of the SELP Library. Two SELP sequences (SE_{AI} and bSE_{AI}) were designed (Table 1). SE_{AI} was formed entirely by structural silk-like blocks (GAGAGS) or elastin-like blocks (IPAVG, VPGVG, and VPGIG), whereas bSE_{AI} also contained a functional domain capable of biomineralizing hydroxyapatite (VTKHLNQISQSY). Synthetic DNA sequences encoding for the full length of the SELPs were purchased from GeneArt (Regensburg, Germany). Plasmids containing the SELP genes were then transformed into an electrocompetent *E. coli* K12 strain proprietary of DSM (Delft, The Netherlands). Successful transformants were randomly selected and used for bacterial fermentation in 2-L shake flasks containing 500 mL of Terrific Broth medium. Cultivation was performed at 37 °C and cells were induced with L-arabinose when the optical density of the culture at 600 nm reached 0.6. Cells were harvested 4 h after induction by centrifugation at 5500 rcf for 20 min at 4 °C. The supernatant was decanted, and the cell pellets were subjected to a freeze−thaw cycle to rupture them. Thereafter, cell pellets were resuspended in Milli-Q water, and the pH adjusted to 4 to prevent the cleavage by proteases. This was especially relevant for bSE_{AI}, because bioactive domains can sometimes exhibit degradation by proteases.[14] The resulting suspension was then tip sonicated on ice to release the SELPs. The LCST behavior of SELPs allowed for their purification via a simple nonchromatographic method called inverse temperature cycling, alternating between the one- and two-phase regime of their phase diagram.[14,58] The phase-separation of SELPs was triggered by adding 2 M NaCl and incubating the solutions at 42 °C. The duration of the incubation step at 42 °C was kept to a minimum (until turbidity was observed in the solution) to reduce the formation of irreversible β-sheets between silk blocks, as these could turn the SELPs insoluble.

Purified SELPs were desalted in 3000 MWCO Amicon ultra-15 centrifugal filter units (MilliporeSigma). The desalted materials were then resuspended in Milli-Q water, flash-frozen and lyophilized, followed by storage at −20 °C until further use. The theoretical hydrophobicity of the SELPs was calculated using the Kyte-Doolittle scale.[56]

Protein Characterization. *Molecular Weight (MW) Determination.* The average molecular weight of SELPs was determined via reversed phase LC-HRMS[59] (Figure S12).

Sodium Dodecyl Sulfate−Polyacrylamide Gel Electrophoresis (SDSPAGE). SDS PAGE was performed using NuPAGE 4−12% Bis-tris gels (Invitrogen). Mark12 unstained standard (Thermo Fisher) was used as protein ladder. Gels were stained using SYPRO Red gel staining agent (Invitrogen) following the manufacturer's protocol.

NMR Spectroscopy. Lyophilized SELPs were dissolved in deuterated water (D_2O) to a concentration of 50 mg/mL. NMR spectra of the natural abundance nuclei were recorded at 295 K on a 700 MHz spectrometer equipped with cryogenic probe. For the 1D

spectrum excitation sculpting was used to suppress residual water. For the 2D $^1H−^{13}C$ correlation spectra a multiplicity edited sensitivity enhanced HSQC was applied using Echo/Antiecho-TPPI for phase selection.

Protein Formulations. Purified SE_{AI} and bSE_{AI} were used in three different formulations (untreated, postprocessing via water vapor annealing, and postprocessing via EtOH annealing). These formulations led to different contents in intermolecular β-sheet physical cross-links via the silk-like blocks.

Untreated. SELPs were used as obtained after purification and freeze-drying.

Water Vapor Annealing. Freeze-dried SELPs were subjected to water vapor annealing by placing them in a vacuum chamber along with a shallow Petri dish containing 250 mL of distilled water. The SELPs did not directly contact the water. The vacuum chamber pressure was lowered to 13 mbar to create a humid environment inside the chamber at room temperature and kept overnight under those conditions. Afterward, the water-annealed SELPs were air-dried in a fume hood, cryo-milled, and stored in a closed container at −20 °C until further use.

Ethanol Annealing. Freeze-dried SELPs were submerged in absolute ethanol at room temperature and placed in a rolling bench overnight. Afterward, EtOH was discarded and the EtOH-annealed material was air-dried in a fume hood, cryo-milled, and stored in a closed container at −20 °C until further use.

Hydrogel Formation and Characterization. *Rheology.* Rheological characterization was performed to assess the ability of SELP solutions to form hydrogels, and to characterize their viscoelastic properties. Dry SELPs in each formulation (untreated, after water vapor annealing, or after EtOH annealing) were dissolved in cold Milli-Q water at a concentration of 15 wt %. Small amplitude oscillatory shear rheology measurements were performed on a stress-controlled rheometer (Anton Paar MCR 301) using a cone−plate geometry with a diameter of 50 mm and a cone angle of 1°. The temperature was controlled by a Peltier system. For each test, 590 μL of freshly prepared SELP solutions were loaded at 4 °C onto the bottom plate using a pipet, followed by equilibration for 5 min. Low viscosity mineral oil (Sigma-Aldrich) was applied to the air-sample interface around the measuring geometry to prevent water evaporation. The LCST-like behavior of SELP solutions was analyzed with a temperature sweep between 4 and 37 °C (with a rate of 1 °C/min). The reversibility of gelation was assessed with three temperature cycles between 4 and 37 °C (with a rate of 1 °C/min). Holding times of 30 min were applied at 4 and 37 °C, after each temperature ramp. Strain sweeps were performed from 0.01% to 15% at a frequency of 1 Hz to evaluate the linear viscoelastic region of these hydrogels. Frequency sweeps were carried out at 4 and 37 °C from 0.1 to 100 rad/s, using a constant strain of 0.3%. Additional rheological measurements were done to separate the influence on the mechanical properties of β-sheets from those owed purely to biopolymer entanglements. To that end, 15 wt % solutions of SELPs in 6 M solutions of guanidinium chloride (GdmCl) in Milli-Q water were used.

Fourier Transform Infrared Spectroscopy (FTIR). Dry SELPs were analyzed by FTIR to assess their secondary structure in the dry state for the different formulations. Infrared spectra were measured in a Bruker Vertex 70 Attenuated Total Reflectance FTIR device equipped with a Harrick split pea accessory. For each measurement, 64 scans with a resolution of 2 cm^{-1} were recorded in the range of 650 to 4000 cm^{-1}.

Dynamic Light Scattering (DLS). The hydrodynamic diameter of SELPs in solution (0.5 mg/mL) was measured using a Zetasizer Nano Series dynamic light scattering (DLS) instrument (Malvern Instruments). Samples were dissolved in water and incubated at 4 °C for 1 h. Subsequently, they were filtered using a 0.2 μm syringe filter prior to analysis. Measurements were performed in plastic polystyrene cuvettes (BrandTech Scientific) at 25 °C. The laser power was adjusted automatically by the built-in autoattenuation capability for each sample to an optimized range of counts. The acquisition time for each data point was 10 s, and 5 measurements were performed for

each sample. The theoretical hydrodynamic diameter was estimated using the formula $D_h^{IDP} = 4.66N^{0.549}$, where N is the number of amino acids for each SELP (432 for SE_{AI} and 468 for bSE_{AI}).[60]

Differential Scanning Calorimetry (DSC). DSC experiments were carried out in a Mettler Toledo DSC1 device using hermetically sealed aluminum pans. For each sample, a volume of 40 μL of SELP solution (15 wt %) was used. Samples were dissolved in water and incubated at 4 °C for 1 h. Subsequently, samples were subjected to 3 temperature cycles (30 min isotherm at 4 °C, heating ramp from for to 50 °C with a heating rate of 1 °C/min, 30 min isotherm at 50 °C and a cooling ramp of 1 °C/min down to 4 °C).

Small-Angle X-ray Scattering (SAXS) and Wide-Angle X-ray Scattering (WAXS). SAXS and WAXS experiments were performed using a SAXSLAB Ganesha 300XL (Xenocs) microfocus X-ray tube with copper radiation with a motorized collimation system. Dry SELP samples were mounted on tape holders and placed in an evacuated chamber at 0.08 mbar. The scattered intensity was collected by a solid-state photon-counting Pilatus 300 K (Dectris, Switzerland) detector. The sample−detector distance was set to 1041 mm for SAXS measurements and 101 mm for WAXS measurements. The acquisition time was 1800 s for SAXS measurements and 300 s for WAXS measurements. Background signals from empty tape holders were subtracted from each measurement before data analysis. The obtained 2D images were background-corrected, azimuthally averaged, and plotted as 1D scattering profiles using SAXSGUI software.

Atomic Force Microscopy (AFM). Samples for AFM imaging were prepared by diluting dry SELPs in cold Milli-Q water to a final concentration of 0.1 μg/mL. Thereafter, 5 μL of solution were deposited onto a freshly cleaved mica. The sample was left to dry overnight at 4 °C to reduce the thermal motion of SELPs and thus prevent protein aggregation due to rapid evaporation of the aqueous solvent. Samples were subsequently imaged in air using an Icon AFM (Bruker) with ScanAsyst-Air-HPI tips. The AFM was operated using the ScanAsyst Tapping mode at room conditions. The scan area was set to 1×1 μm² or 5×5 μm², and images were recorded at 512×512 pixels and a line rate of 1 Hz. A second-order flattening was performed on all images using NanoScope Analysis 10.0 software.

Scanning Electron Microscopy (SEM). Dry SELPs in different formulations were analyzed by SEM to investigate their microstructure. Samples were coated with a layer of Au/Pd using a SC7620 mini Sputter Coater/Glow Discharge System (Quorum Technologies). SEM images were obtained using a Zeiss GeminiSEM 360 microscope with in-lens detector.

Computational Simulations. Molecular dynamics (MD) simulations were used to study the interaction between SELPs at the atomistic level. Input structures for MD simulations were created with the SELP sequences shown in Table 1. Extended conformations of each SELP were built using the software Avogadro (version 1.2.0).[61] MD simulations were performed in Gromacs (2021.2 version)[62] using the CHARMM36m force field.[63] The atomic structures were visualized using the Visual Molecular Dynamics (VMD) graphics software.[64]

Implicit Solvent Simulations. Each extended SELP structure was subjected to MD simulations in implicit solvent to obtain a folded structure. The equilibration and folding of SELPs was assessed by the evolution of the root mean squared displacement (RMSD) of their atomic positions. First, the structure was subjected to energy minimization for 50,000 timesteps to relax the polypeptide, using the steepest descent algorithm. This was followed by an implicit solvent run at 400 K using a simulation step of 1 fs for a total simulation time of 50 ns. The aim of these simulations was to speed up the folding of the SELP molecules into compact structures to be used in subsequent explicit solvent simulations.

Explicit Solvent Simulations. Two copies of the final structures obtained in implicit solvent simulations were solvated in a TIP3P water box with 3D periodic boundary conditions to a final concentration of ca. 150 mg/mL. For bSE_{AI}, the charge of the biomineralizing block was neutralized by adding the required NaCl ions. The LINC algorithm was applied to all the bonds containing hydrogen atoms. The resulting systems were equilibrated by subjecting them to energy minimization for 50,000 timesteps, 100 ps using the NVT ensemble at 310 K using a Nosé−Hoover temperature coupling, and 100 ps using the NPT ensemble at 310 K with Parrinello−Rahman pressure coupling. The resulting equilibrated systems were subjected to replica exchange molecular dynamics (REMD). 80 replicas in explicit solvent were used, with temperatures exponentially distributed from 280 to 380 K. A time step of 2 fs was applied, and each replica was simulated for 50 ns, with exchange attempts every 2 ps. The long-range electrostatic Coulombic interactions were calculated using particle mesh Ewald method with a grid spacing of 1.6 Å. A cutoff distance of 10 Å was applied for electrostatic and van der Waals interactions.

Data Analysis. A low temperature (7 °C) and a high temperature (37 °C) replicas were subjected to further analysis, to understand the differences in the dynamics of the interaction between SE_{AI} and bSE_{AI}. Molecular properties were sampled for the last 10% of the MD trajectories. The package MDAnalysis[65,66] was used to analyze the number of intermolecular contacts, the intra/interprotein and protein−water hydrogen bonding patterns, the RMSD of the atomic positions, and the radial distribution function. The solvent accessible surface area (SASA), secondary structure, interaction energies and number of water molecules in the solvation shell were calculated using the GROMACS tools gmx sasa, gmx dssp, gmx energy and gmx select, respectively. The distance for the first valley of the RDFs was used as a cutoff to compute the solvation shell (Figure S13).

■ ASSOCIATED CONTENT

Ⓢ Supporting Information

The Supporting Information is available free of charge at https://pubs.acs.org/doi/10.1021/acsami.4c17903.

Additional NMR spectra, SDS PAGE gels, additional rheological characterization, full FTIR spectra, AFM images of different SELP samples at different magnifications, SAXS/WAXS 2D patterns, LC-HRMS chromatograms and radial distribution function of water molecules in MD simulations (PDF)

■ AUTHOR INFORMATION

Corresponding Author

Diego López Barreiro − *Manufacturing Futures Lab, Department of Chemical Engineering and Centre for Nature-Inspired Engineering, Department of Chemical Engineering, University College London, London WC1E 7JE, United Kingdom; dsm-firmenich Science & Research, Biotechnology, Delft 2613 AX, The Netherlands;* ⓞ orcid.org/0000-0002-9346-655X; Email: d.lopezbarreiro@ucl.ac.uk

Authors

Klaartje Houben − *dsm-firmenich Science & Research, Analytical Sciences, Delft 2613 AX, The Netherlands;* ⓞ orcid.org/0000-0002-6221-2987

Olaf Schouten − *dsm-firmenich Science & Research, Analytical Sciences, Delft 2613 AX, The Netherlands*

Gijsje H. Koenderink − *Department of Bionanoscience, Kavli Institute of Nanoscience Delft, Delft University of Technology, Delft 2629 HZ, The Netherlands;* ⓞ orcid.org/0000-0002-7823-8807

Jens C. Thies − *DSM Biomedical, Geleen 6160 BB, The Netherlands*

Cees M. J. Sagt − *dsm-firmenich Science & Research, Biotechnology, Delft 2613 AX, The Netherlands*

Complete contact information is available at:
https://pubs.acs.org/10.1021/acsami.4c17903

■ REFERENCES

(1) Harrington, M. J.; Fratzl, P. Natural load-bearing protein materials. *Prog. Mater. Sci.* **2021**, *120*, No. 100767.

(2) Miserez, A.; Yu, J.; Mohammadi, P. Protein-Based Biological Materials: Molecular Design and Artificial Production. *Chem. Rev.* **2023**, *123* (5), 2049−2111.

(3) Harrington, M. J.; Mezzenga, R.; Miserez, A. Fluid protein condensates for bio-inspired applications. *Nature Reviews Bioengineering* **2024**, *2* (3), 260−278.

(4) Huang, W.; Ling, S.; Li, C.; Omenetto, F. G.; Kaplan, D. L. Silkworm silk-based materials and devices generated using bio-nanotechnology. *Chem. Soc. Rev.* **2018**, *47* (17), 6486−6504.

(5) Marelli, B.; Brenckle, M. A.; Kaplan, D. L.; Omenetto, F. G. Silk Fibroin as Edible Coating for Perishable Food Preservation. *Sci. Rep.* **2016**, *6* (1), 25263.

(6) Matzeu, G.; Mogas-Soldevila, L.; Li, W.; Naidu, A.; Turner, T. H.; Gu, R.; Blumeris, P. R.; Song, P.; Pascal, D. G.; Guidetti, G.; et al. Large-Scale Patterning of Reactive Surfaces for Wearable and Environmentally Deployable Sensors. *Adv. Mater.* **2020**, *32* (28), No. 2001258.

(7) Lee, A.; Hudson, A. R.; Shiwarski, D. J.; Tashman, J. W.; Hinton, T. J.; Yerneni, S.; Bliley, J. M.; Campbell, P. G.; Feinberg, A. W. 3D bioprinting of collagen to rebuild components of the human heart. *Science* **2019**, *365* (6452), 482−487.

(8) Ling, S.; Qin, Z.; Huang, W.; Cao, S.; Kaplan, D. L.; Buehler, M. J. Design and function of biomimetic multilayer water purification membranes. *Science Advances* **2017**, *3* (4), No. e1601939.

(9) Liu, Y.; Gilchrist, A. E.; Heilshorn, S. C. Engineered Protein Hydrogels as Biomimetic Cellular Scaffolds. *Adv. Mater.* **2024**, *36* (45), 2407794.

(10) Yang, Y. J.; Holmberg, A. L.; Olsen, B. D. Artificially Engineered Protein Polymers. *Annu. Rev. Chem. Biomol. Eng.* **2017**, *8* (1), 549−575.

(11) El Maachi, I.; Loewen, A.; Acosta, S.; Rütten, S.; Rodríguez-Cabello, J. C.; Jockenhoevel, S.; Fernández-Colino, A. Protein-Engineered Elastin Fibers as Building Blocks for The Textile-Based Assembly of Tissue Equivalents. *Adv. Funct. Mater.* **2024**, *34* (24), No. 2313204.

(12) Urry, D. W.; Long, M. M.; Cox, B. A.; Ohnishi, T.; Mitchell, L. W.; Jacobs, M. The synthetic polypentapeptide of elastin coacervates and forms filamentous aggregates. *Biochimica et Biophysica Acta (BBA) - Protein Structure* **1974**, *371* (2), 597−602.

(13) López Barreiro, D.; Minten, I. J.; Thies, J. C.; Sagt, C. M. J. Structure−Property Relationships of Elastin-like Polypeptides: A Review of Experimental and Computational Studies. *ACS Biomaterials Science & Engineering* **2023**, *9* (7), 3796−3809.

(14) Rodríguez-Cabello, J. C.; Girotti, A.; Ribeiro, A.; Arias, F. J. Synthesis of Genetically Engineered Protein Polymers (Recombi-

namers) as an Example of Advanced Self-Assembled Smart Materials. In *Nanotechnology in Regenerative Medicine: Methods and Protocols*, Navarro, M.; Planell, J. A., Eds.; Humana Press: 2012; pp 17−38.

(15) Ling, S.; Li, C.; Adamcik, J.; Shao, Z.; Chen, X.; Mezzenga, R. Modulating Materials by Orthogonally Oriented β-Strands: Composites of Amyloid and Silk Fibroin Fibrils. *Adv. Mater.* **2014**, *26* (26), 4569−4574.

(16) Huang, W.; Tarakanova, A.; Dinjaski, N.; Wang, Q.; Xia, X.; Chen, Y.; Wong, J. Y.; Buehler, M. J.; Kaplan, D. L. Design of Multistimuli Responsive Hydrogels Using Integrated Modeling and Genetically Engineered Silk−Elastin-Like Proteins. *Adv. Funct. Mater.* **2016**, *26* (23), 4113−4123.

(17) Qiu, W.; Huang, Y.; Teng, W.; Cohn, C. M.; Cappello, J.; Wu, X. Complete Recombinant Silk-Elastinlike Protein-Based Tissue Scaffold. *Biomacromolecules* **2010**, *11* (12), 3219−3227.

(18) Gustafson, J. A.; Price, R. A.; Greish, K.; Cappello, J.; Ghandehari, H. Silk-Elastin-like Hydrogel Improves the Safety of Adenovirus-Mediated Gene-Directed Enzyme−Prodrug Therapy. *Mol. Pharmaceutics* **2010**, *7* (4), 1050−1056.

(19) Isaacson, K. J.; Jensen, M. M.; Watanabe, A. H.; Green, B. E.; Correa, M. A.; Cappello, J.; Ghandehari, H. Self-Assembly of Thermoresponsive Recombinant Silk-Elastinlike Nanogels. *Macromol. Biosci.* **2018**, *18* (1), No. 1700192.

(20) Wang, E.; Desai, M. S.; Lee, S.-W. Light-Controlled Graphene-Elastin Composite Hydrogel Actuators. *Nano Lett.* **2013**, *13* (6), 2826−2830.

(21) Parker, R. N.; Wu, W. A.; McKay, T. B.; Xu, Q.; Kaplan, D. L. Design of Silk-Elastin-Like Protein Nanoparticle Systems with Mucoadhesive Properties. *Journal of Functional Biomaterials* **2019**, *10* (4), 49.

(22) Huang, W.; Rollett, A.; Kaplan, D. L. Silk-elastin-like protein biomaterials for the controlled delivery of therapeutics. *Expert Opinion on Drug Delivery* **2015**, *12* (5), 779−791.

(23) Cipriani, F.; Krüger, M.; de Torre, I. G.; Sierra, L. Q.; Rodrigo, M. A.; Kock, L.; Rodriguez-Cabello, J. C. Cartilage Regeneration in Preannealed Silk Elastin-Like Co-Recombinamers Injectable Hydrogel Embedded with Mature Chondrocytes in an Ex Vivo Culture Platform. *Biomacromolecules* **2018**, *19* (11), 4333−4347.

(24) Ibáñez-Fonseca, A.; Orbanic, D.; Arias, F. J.; Alonso, M.; Zeugolis, D. I.; Rodríguez-Cabello, J. C. Influence of the Thermodynamic and Kinetic Control of Self-Assembly on the Microstructure Evolution of Silk-Elastin-Like Recombinamer Hydrogels. *Small* **2020**, *16* (28), No. 2001244.

(25) López Barreiro, D.; Folch-Fortuny, A.; Muntz, I.; Thies, J. C.; Sagt, C. M. J.; Koenderink, G. H. Sequence Control of the Self-Assembly of Elastin-Like Polypeptides into Hydrogels with Bespoke Viscoelastic and Structural Properties. *Biomacromolecules* **2023**, *24* (1), 489−501.

(26) Fernández-Colino, A.; Arias, F. J.; Alonso, M.; Rodríguez-Cabello, J. C. Amphiphilic Elastin-Like Block Co-Recombinamers Containing Leucine Zippers: Cooperative Interplay between Both Domains Results in Injectable and Stable Hydrogels. *Biomacromolecules* **2015**, *16* (10), 3389−3398.

(27) Jung, H.; Pena-Francesch, A.; Saadat, A.; Sebastian, A.; Kim, D. H.; Hamilton, R. F.; Albert, I.; Allen, B. D.; Demirel, M. C. Molecular tandem repeat strategy for elucidating mechanical properties of high-strength proteins. *Proc. Natl. Acad. Sci. U. S. A.* **2016**, *113* (23), 6478−6483.

(28) Rombouts, W. H.; de Kort, D. W.; Pham, T. T. H.; van Mierlo, C. P. M.; Werten, M. W. T.; de Wolf, F. A.; van der Gucht, J. Reversible Temperature-Switching of Hydrogel Stiffness of Coassembled, Silk-Collagen-Like Hydrogels. *Biomacromolecules* **2015**, *16* (8), 2506−2513.

(29) Dzuricky, M.; Rogers, B. A.; Shahid, A.; Cremer, P. S.; Chilkoti, A. De novo engineering of intracellular condensates using artificial disordered proteins. *Nat. Chem.* **2020**, *12* (9), 814−825.

(30) Li, N. K.; Roberts, S.; Quiroz, F. G.; Chilkoti, A.; Yingling, Y. G. Sequence Directionality Dramatically Affects LCST Behavior of

Elastin-Like Polypeptides. *Biomacromolecules* **2018**, *19* (7), 2496−2505.

(31) Rauscher, S.; Pomès, R. The liquid structure of elastin. *eLife* **2017**, *6*, No. e26526.

(32) Glassman, M. J.; Olsen, B. D. Arrested Phase Separation of Elastin-like Polypeptide Solutions Yields Stiff. *Thermoresponsive Gels. Biomacromolecules* **2015**, *16* (12), 3762−3773.

(33) Segvich, S. J.; Smith, H. C.; Kohn, D. H. The adsorption of preferential binding peptides to apatite-based materials. *Biomaterials* **2009**, *30* (7), 1287−1298.

(34) Meyer, D. E.; Chilkoti, A. Purification of recombinant proteins by fusion with thermally-responsive polypeptides. *Nat. Biotechnol.* **1999**, *17* (11), 1112−1115.

(35) https://bmrb.io/histogram/ (accessed 2024 17/05/2024).

(36) Wang, Y.; Jardetzky, O. Probability-based protein secondary structure identification using combined NMR chemical-shift data. *Protein Sci.* **2002**, *11* (4), 852−861.

(37) Theillet, F.-X.; Kalmar, L.; Tompa, P.; Han, K.-H.; Selenko, P.; Dunker, A. K.; Daughdrill, G. W.; Uversky, V. N. The alphabet of intrinsic disorder. *Intrinsically Disordered Proteins* **2013**, *1* (1), No. e24360.

(38) Sebák, F.; Szolomájer, J.; Papp, N.; Tóth, G. K.; Bodor, A. Proline cis/trans Isomerization in Intrinsically Disordered Proteins and Peptides. *Front. Biosci. (Landmark Ed.)* **2023**, *28* (6), 127.

(39) Hu, X.; Shmelev, K.; Sun, L.; Gil, E.-S.; Park, S.-H.; Cebe, P.; Kaplan, D. L. Regulation of Silk Material Structure by Temperature-Controlled Water Vapor Annealing. *Biomacromolecules* **2011**, *12* (5), 1686−1696.

(40) Chen, X.; Knight, D. P.; Shao, Z.; Vollrath, F. Regenerated Bombyx silk solutions studied with rheometry and FTIR. *Polymer* **2001**, *42* (25), 09969−09974.

(41) Cao, Y.; Li, H. How Do Chemical Denaturants Affect the Mechanical Folding and Unfolding of Proteins? *J. Mol. Biol.* **2008**, *375* (1), 316−324.

(42) Garanger, E.; MacEwan, S. R.; Sandre, O.; Brûlet, A.; Bataille, L.; Chilkoti, A.; Lecommandoux, S. Structural Evolution of a Stimulus-Responsive Diblock Polypeptide Micelle by Temperature Tunable Compaction of its Core. *Macromolecules* **2015**, *48* (18), 6617−6627.

(43) Gonzalez-Obeso, C.; Rodriguez-Cabello, J. C.; Kaplan, D. L. Fast and reversible crosslinking of a silk elastin-like polymer. *Acta Biomaterialia* **2022**, *141*, 14−23.

(44) Hu, X.; Kaplan, D.; Cebe, P. Determining Beta-Sheet Crystallinity in Fibrous Proteins by Thermal Analysis and Infrared Spectroscopy. *Macromolecules* **2006**, *39* (18), 6161−6170.

(45) Morozova, S.; Hitimana, E.; Dhakal, S.; Wilcox, K. G.; Estrin, D. Scattering methods for determining structure and dynamics of polymer gels. *J. Appl. Phys.* **2021**, *129* (7), No. 071101.

(46) Cao, Y.; Olsen, B. D. Strengthening and Toughening of Protein-Based Thermosets via Intermolecular Self-Assembly. *Biomacromolecules* **2022**, *23* (8), 3286−3295.

(47) Yazawa, K.; Ishida, K.; Masunaga, H.; Hikima, T.; Numata, K. Influence of Water Content on the *β*-Sheet Formation, Thermal Stability, Water Removal, and Mechanical Properties of Silk Materials. *Biomacromolecules* **2016**, *17* (3), 1057−1066.

(48) Sun, H.; Marelli, B. Polypeptide templating for designer hierarchical materials. *Nat. Commun.* **2020**, *11* (1), 351.

(49) Li, J.; Zhu, Y.; Yu, H.; Dai, B.; Jun, Y.-S.; Zhang, F. Microbially Synthesized Polymeric Amyloid Fiber Promotes *β*-Nanocrystal Formation and Displays Gigapascal Tensile Strength. *ACS Nano* **2021**, *15* (7), 11843−11853.

(50) Chan, W. Y.; Bochenski, T.; Schmidt, J. E.; Olsen, B. D. Peptide Domains as Reinforcement in Protein-Based Elastomers. *ACS Sustainable Chem. Eng.* **2017**, *5* (10), 8568−8578.

(51) Mithieux, S. M.; Aghaei-Ghareh-Bolagh, B.; Yan, L.; Kuppan, K. V.; Wang, Y.; Garces-Suarez, F.; Li, Z.; Maitz, P. K.; Carter, E. A.; Limantoro, C.; et al. Tropoelastin Implants That Accelerate Wound Repair. *Adv. Healthcare Mater.* **2018**, *7* (10), No. 1701206.

(52) Xiao, Y.; Liu, Y.; Zhang, W.; Qi, P.; Ren, J.; Pei, Y.; Ling, S. Formation, Structure, and Mechanical Performance of Silk Nanofibrils Produced by Heat-Induced Self-Assembly. *Macromol. Rapid Commun.* **2021**, *42* (3), No. 2000435.

(53) Nguyen, A. T.; Huang, Q.-L.; Yang, Z.; Lin, N.; Xu, G.; Liu, X. Y. Crystal Networks in Silk Fibrous Materials: From Hierarchical Structure to Ultra Performance. *Small* **2015**, *11* (9−10), 1039−1054.

(54) Adamcik, J.; Mezzenga, R. Amyloid Polymorphism in the Protein Folding and Aggregation Energy Landscape. *Angew. Chem., Int. Ed.* **2018**, *57* (28), 8370−8382.

(55) Mu, X.; Yuen, J. S. K.; Choi, J.; Zhang, Y.; Cebe, P.; Jiang, X.; Zhang, Y. S.; Kaplan, D. L. Conformation-driven strategy for resilient and functional protein materials. *Proc. Natl. Acad. Sci. U. S. A.* **2022**, *119* (4), No. e2115523119.

(56) Kamada, A.; Rodriguez-Garcia, M.; Ruggeri, F. S.; Shen, Y.; Levin, A.; Knowles, T. P. J. Controlled self-assembly of plant proteins into high-performance multifunctional nanostructured films. *Nat. Commun.* **2021**, *12* (1), 3529.

(57) Pena-Francesch, A.; Jung, H.; Demirel, M. C.; Sitti, M. Biosynthetic self-healing materials for soft machines. *Nat. Mater.* **2020**, *19* (11), 1230−1235.

(58) Varanko, A. K.; Su, J. C.; Chilkoti, A. Elastin-Like Polypeptides for Biomedical Applications. *Annu. Rev. Biomed. Eng.* **2020**, *22* (1), 343−369.

(59) Vente, A.; Mladic, M.; López Barreiro, D.; Schouten, O.; van der Hoeven, R. *Characterization of elastin-like polypeptides combining a novel proalanase bottom-up approach and intact protein analysis*; IMSC: Maastricht, the Netherlands, 2022.

(60) Marsh, J. A.; Forman-Kay, J. D. Sequence Determinants of Compaction in Intrinsically Disordered Proteins. *Biophys. J.* **2010**, *98* (10), 2383−2390.

(61) Hanwell, M. D.; Curtis, D. E.; Lonie, D. C.; Vandermeersch, T.; Zurek, E.; Hutchison, G. R. Avogadro: an advanced semantic chemical editor, visualization, and analysis platform. *Journal of Cheminformatics* **2012**, *4* (1), 17.

(62) Abraham, M. J.; Murtola, T.; Schulz, R.; Páll, S.; Smith, J. C.; Hess, B.; Lindahl, E. GROMACS: High performance molecular simulations through multi-level parallelism from laptops to super-computers. *SoftwareX* **2015**, *1−2*, 19−25.

(63) Huang, J.; Rauscher, S.; Nawrocki, G.; Ran, T.; Feig, M.; de Groot, B. L.; Grubmüller, H.; MacKerell, A. D. CHARMM36m: an improved force field for folded and intrinsically disordered proteins. *Nat. Methods* **2017**, *14* (1), 71−73.

(64) Humphrey, W.; Dalke, A.; Schulten, K. VMD: Visual molecular dynamics. *J. Mol. Graphics* **1996**, *14* (1), 33−38.

(65) Michaud-Agrawal, N.; Denning, E. J.; Woolf, T. B.; Beckstein, O. MDAnalysis: A toolkit for the analysis of molecular dynamics simulations. *J. Comput. Chem.* **2011**, *32* (10), 2319−2327.

(66) Gowers, R. J.; Linke, M.; Barnoud, J.; Reddy, T. J. E.; Melo, M. N.; Seyler, S. L.; Domański, J.; Dotson, D. L.; Buchoux, S.; Kenney, I. M.; Beckstein, O. MDAnalysis: A Python Package for the Rapid Analysis of Molecular Dynamics Simulations. In *Proceedings of the Python in Science Conference*; Benthall, S.; Rostrup, S., Eds.; 2016; pp 98-105. DOI: https://www.doi.org/10.25080/Majora-629e541a-00e.